Journal of
Applied Crystallography
ISSN 0021-8898

Received 8 December 2009
Accepted 8 March 2010

Enhancement of second harmonic generation, optical and dielectric properties in L-asparagine monohydrate single crystals due to an improvement in crystalline perfection by annealing

Mohd. Shakir,[a,b] S. K. Kushawaha,[a] K. K. Maurya,[a] Sumeet Kumar,[a] M. A. Wahab[b] and G. Bhagavannarayana[a]*

[a]Materials Characterization Division, National Physical Laboratory, Council of Scientific and Industrial Research, New Delhi 110 012, India, and [b]Crystal Growth Laboratory, Department of Physics, Jamia Millia Islamia, New Delhi 110025, India. Correspondence e-mail: bhagavan@mail.nplindia.ernet.in

Single crystals of the relatively new nonlinear optical material L-asparagine monohydrate have been successfully grown by the slow evaporation solution growth technique at room temperature in aqueous solution. The crystal system of the title material has been confirmed by powder X-ray diffraction. The crystalline perfection of the as-grown and annealed crystals has been evaluated by high-resolution X-ray diffraction. The as-grown single crystals (particularly when their size is large) were found to contain internal structural grain boundaries, and the crystalline perfection of these crystals was found to be improved substantially by annealing at low temperatures. The crystalline perfection and the measured physical properties were found to be correlated such that the second harmonic generation efficiency, optical transparency, fluorescence and dielectric properties are enhanced as the crystal quality improves.

1. Introduction

The design of devices that utilize photons instead of electrons in data retrieval, storage, processing and transmission has created a need for new materials with unique optical properties (Williams, 1984). In recent years, nonlinear optical (NLO) materials have attracted much attention because of their widespread application in high-energy lasers for inertial confinement fusion research (Zaitseva & Carman, 2001), color displays, electro-optic switches, frequency conversion *etc.* (Badan *et al.*, 1993).

Many of the direction-dependent physical and optical properties of these materials can deteriorate or be significantly diminished when they are not in the single-crystal domain or have defects such as structural grain boundaries (Bhagavannarayana, Ananthamurthy *et al.*, 2005; Bhagavannarayana, Budakoti *et al.*, 2005). It therefore becomes very important to assess the crystalline perfection, second harmonic generation (SHG) efficiency, and optical and dielectric properties of grown single crystals to ascertain their suitability for device applications.

Many organic compounds show good NLO properties owing to the presence of active π bonds, which help in the molecular engineering of tailor-made applications. In particular, the family of organic or semiorganic amino acids shows interesting NLO properties (Pan *et al.*, 2007; Misoguti *et al.*, 1996). L-Asparagine monohydrate (LAM) is an organic compound from this family. Among other biological substances, asparagine is a very important amino acid because it plays a role in the metabolic control of some cell functions in nerve and brain tissues, and is also used by many plants as a nitrogen reserve source (Lund, 1981).

LAM crystallizes in the orthorhombic structure having space group $P2_12_12_1$ with four molecules per unit cell and lattice parameters $a = 5.593$, $b = 9.827$, $c = 11.808$ Å (Verbist *et al.*, 1972). Electron paramagnetic resonance (EPR) and optical absorption studies of VO^{2+} ions in LAM have been conducted at room temperature (Kripal & Singh, 2007*a*). The incorporation of Mn^{2+} and elastic distortion in the crystalline lattice of LAM have also been studied by EPR and optical absorption (Kripal & Singh, 2007*b*; Krambrock *et al.*, 2007). Polarized first-order Raman scattering studies were carried out in order to obtain the general assignment of the phonon spectra, and a careful analysis of the vibrational spectra shows that the assignment of the fundamental vibrational modes can be achieved on the basis of amine, carboxylic acid and water groups (Moreno *et al.*, 1999). However, to the best of our knowledge there has been no report on the SHG efficiency and optical and dielectric properties of LAM single crystals to date. It is well known that such physical properties of single crystals are very much dependent on crystalline perfection, and annealing is one of the very effective methods that are

used to enhance crystalline perfection (Bhagavannarayana, Ananthamurthy *et al.*, 2005; Bhagavannarayana, Budakoti *et al.*, 2005). Hence, in the present investigation, as-grown LAM single crystals were first subjected to annealing to improve the crystalline perfection, and subsequently the effect of annealing on SHG efficiency and the optical and dielectric properties was studied. The bulk single crystals were grown by the slow evaporation solution technique (SEST) and subjected to powder X-ray diffraction (XRD) to confirm the crystal structure. The crystalline perfection of the as-grown and annealed single crystals has been assessed by high-resolution X-ray diffractometry (HRXRD). The SHG efficiency of the title compound was measured by the Kurtz & Perry (1968) powder technique. Optical studies were performed on as-grown and annealed crystals by fluorescence (FL) and UV–vis spectroscopy. The dielectric properties have been studied *via* an impedance analyzer at various temperatures over a wide range of frequencies.

2. Experimental

2.1. Crystal growth

To grow single crystals of LAM, the commercially available material in powder form (Himedia with 99.8% purity) was taken in a beaker with double-distilled water and left under continuous stirring for 12 h. To avoid the decomposition of the material during this time, the supersaturated solution was kept in a constant-temperature bath (CTB), at the relatively low temperature of 308 K, in a beaker covered with a perforated plastic lid. The temperature of the CTB was reduced slowly to 305 K over a period of 2 d and left for crystal growth by slow evaporation. After 15 d, good size ($10 \times 5 \times 5$ mm) transparent single crystals with natural facets of a particular morphology were harvested. A photograph of a typical as-grown single crystal is shown in Fig. 1. On careful observation, one can see some contrast in the transparency in the middle portion of the crystal, which is clearly visible in almost all of the crystals whose size exceeds a critical value ($\sim 4 \times 2 \times 2$ mm). To obtain a clear understanding about this commonly observed feature, we have carried out HRXRD measurements as described in §3.2.

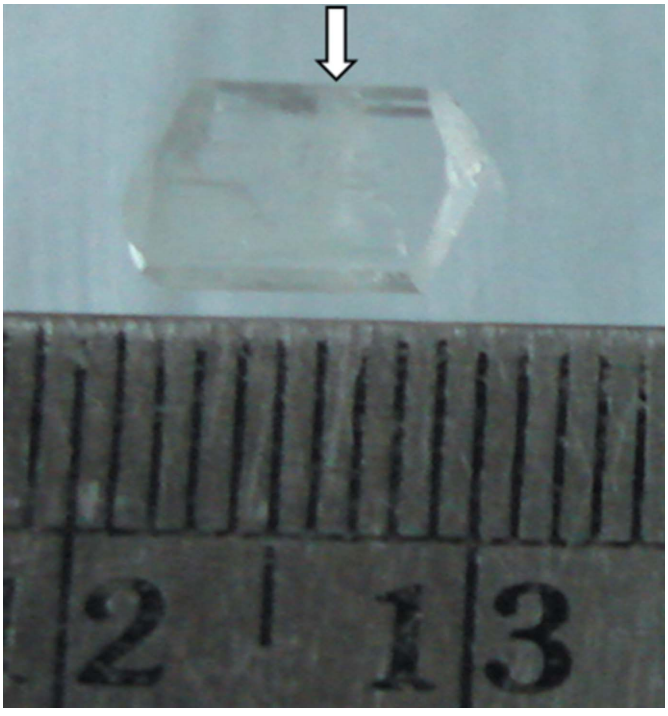

Figure 1
Photograph of a LAM single crystal grown by the SEST method.

2.2. Characterization

To study the crystal system and to determine the lattice parameters, single crystals of LAM were crushed and the fine-powdered sample was subjected to a Bruker D8 ADVANCE powder X-ray diffractometer, employing Cu $K\alpha$ radiation with a graphite monochromator. Powder XRD data were recorded in the angular range 5–70° with a 0.01° s^{-1} scan rate at room temperature.

The crystalline perfection of the as-grown LAM single crystals was characterized using HRXRD by employing a multicrystal X-ray diffractometer designed and developed at the National Physical Laboratory (NPL) (Lal & Bhagavannarayana, 1989). The well collimated and monochromated bMo $K\alpha_1$ beam obtained from three monochromator Si crystals set in a dispersive (+, −, −) configuration was used as the exploratory X-ray beam. The specimen crystal was aligned in the (+, −, −, +) configuration. As a result of the dispersive configuration, though the lattice constant of the monochromator crystal(s) and the specimen are different, the unwanted dispersion broadening in the diffraction curve (DC) of the specimen crystal is insignificant. The specimen can be rotated about the vertical axis, which is perpendicular to the plane of diffraction, with a minimum angular interval of 0.4 arcseconds. The DC was recorded by the so-called ω scan method, wherein the detector was kept at the same angular position $2\theta_B$ with a wide opening for its slit. Before recording the DC, to remove the noncrystallized solute atoms or molecules remaining on the surface of the crystal and also to ensure surface planarity, the specimen was first lapped and chemically etched in a nonpreferential etchant of water and acetone in a 1:2 volume ratio.

To measure the SHG efficiency of the LAM single crystals, well crushed powders of as-grown and annealed crystals were filtered with a 25 µm standard test sieve to achieve a homogeneous particle size. These powders were densely filled in a glass microcapillary of 1 mm bore and subjected to the Kurtz & Perry (1968) powder technique. A standard potassium dihydrogen phosphate (KDP) crystal was used as a reference. A Q-switched Nd:YAG [Spectra Physics (DCR-II)] laser (with a fundamental wavelength of 1064 nm, an input energy of 3.6 mJ $pulse^{-1}$, an 8 ns pulse duration and a repetition rate of 10 Hz with a spot size of 1 mm diameter) was used in 90° scattering geometry as a source. The laser radiation was made incident on the specimen sample, and green output radiation

Table 1
Lattice parameters with standard deviation (σ) of as-grown and annealed LAM single crystals.

Sample	*a*	*b*	*c*
As grown	5.6048	9.8213	11.8143
Annealed at 333 K	5.5932	9.8464	11.8284
Annealed at 353 K	5.6012	9.8563	11.8321
σ	0.0097	0.0147	0.0076

from the specimen was detected by a photomultiplier tube (PMT) coupled with a filter. The signal from the PMT was used to assess the relative SHG efficiency of the grown crystals in comparison to that of the KDP reference crystals.

Optical studies were carried out for as-grown and annealed crystals using a UV–vis spectrophotometer in the 200–1100 nm wavelength range. The fluorescence study was carried out using a Perkin Elmer LS-55 fluorescence spectrofluorometer in the wavelength range 500–800 nm.

To conduct dielectric studies on the LAM crystals, a specimen cut and polished along the [011] direction was subjected to a PSM1735 impedance analyzer. Silver paste was used as electrodes on both sides of the crystal, and the contacts to these electrodes were made by using fine copper wires. The frequency-dependent dielectric constant (ε_r) and dielectric loss ($\tan\delta$) of the specimen were measured in the frequency range 100 Hz–1.0 MHz at temperatures of 303, 313, 333 and 353 K. A home-made furnace with Kanthal wire controlled by a Eurotherm temperature controller with a temperature stability of ± 0.1 K was used for annealing studies. Slow heating and cooling rates of 2–5 K h^{-1} were used to avoid thermal shocks to the crystal.

3. Results and discussion

3.1. Powder X-ray diffraction analysis

The powder X-ray diffraction data recorded for as-grown and annealed LAM crystals are given in Fig. 2. One can clearly see from the figure that the peak intensities and sharpness of the *hkl* planes increase as a result of annealing, showing the enhancement of crystalline perfection with annealing. The 2θ values were taken as the input for lattice-parameter calculation using *PowderX* (Dong, 1999) and *X'Pert HighScore Plus* (PANalytical, Almelo, The Netherlands) and it was confirmed that the grown single crystals belong to the orthorhombic system with space group $P2_12_12_1$. The cell parameters (*a*, *b*, *c*) of the as-grown and annealed samples along with their standard deviations (σ) are given in Table 1. These data are in good agreement with earlier reported data (Verbist *et al.*, 1972).

3.2. High-resolution X-ray diffractometry

Fig. 3(*a*) shows the high-resolution DC recorded for a typical SEST-grown LAM single-crystal specimen in its as-grown state using bMo $K\alpha_1$ radiation in the symmetrical Bragg geometry of the multicrystal X-ray diffractometer described above. The diffracting planes chosen to record the DC are (011). As seen in the figure, the curve contains two diffraction peaks. The solid line, which fits well with the experimental points, is the convoluted curve of the two dotted lines obtained for the Lorentzian fit. The additional peak arises from an internal structural low-angle (tilt angle α greater than 1 arcminutes but less than 1°) grain boundary (Bhagavannarayana, Ananthamurthy *et al.*, 2005) whose tilt angle (misorientation angle between the two crystalline regions on either side of the structural grain boundary) is 98 arcseconds from its adjoining region. The full width at half-maximum (FWHM) of the main peak and the low-angle boundary are, respectively, 25 and 50 arcseconds. The relatively low angular spread of the DC, of around 300 arcseconds, and the low values of FWHM show that the crystalline perfection is fairly good. Indeed, the integrated intensity (area under the curve) of the peak due to the low-angle boundary is much less than that of the main peak, which indicates that the volume of the

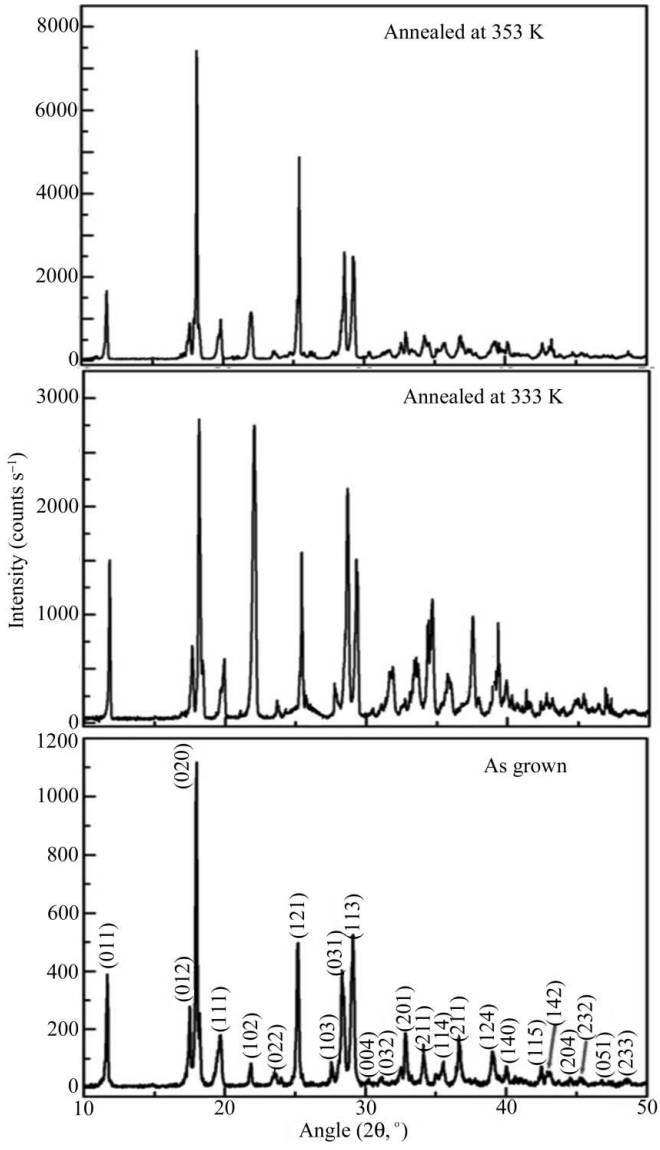

Figure 2
Powder X-ray diffraction patterns of as-grown and annealed LAM crystals.

internal grain boundary is small and the physical properties of the crystal are not much affected by this boundary. In fact, the value of FWHM of the main peak is quite small at 25 arcseconds, which is not very far from that expected by the plane wave theory of dynamical X-ray diffraction (Batterman & Cole, 1964). In SEST-grown crystals it is quite common to observe such low-angle boundaries, which may be due to entrapment of solvent molecules or impurities during crystal growth; these become trapped in the central regions in the form of defect clusters, which in turn lead to grain boundaries (Vijayan *et al.*, 2006, 2007). The fact that the crystalline perfection is not entirely satisfactory is also indicated by the contrast in the transparency as observed in Fig. 1(*a*) The crystals were therefore subjected to annealing at different temperatures to improve the crystal quality.

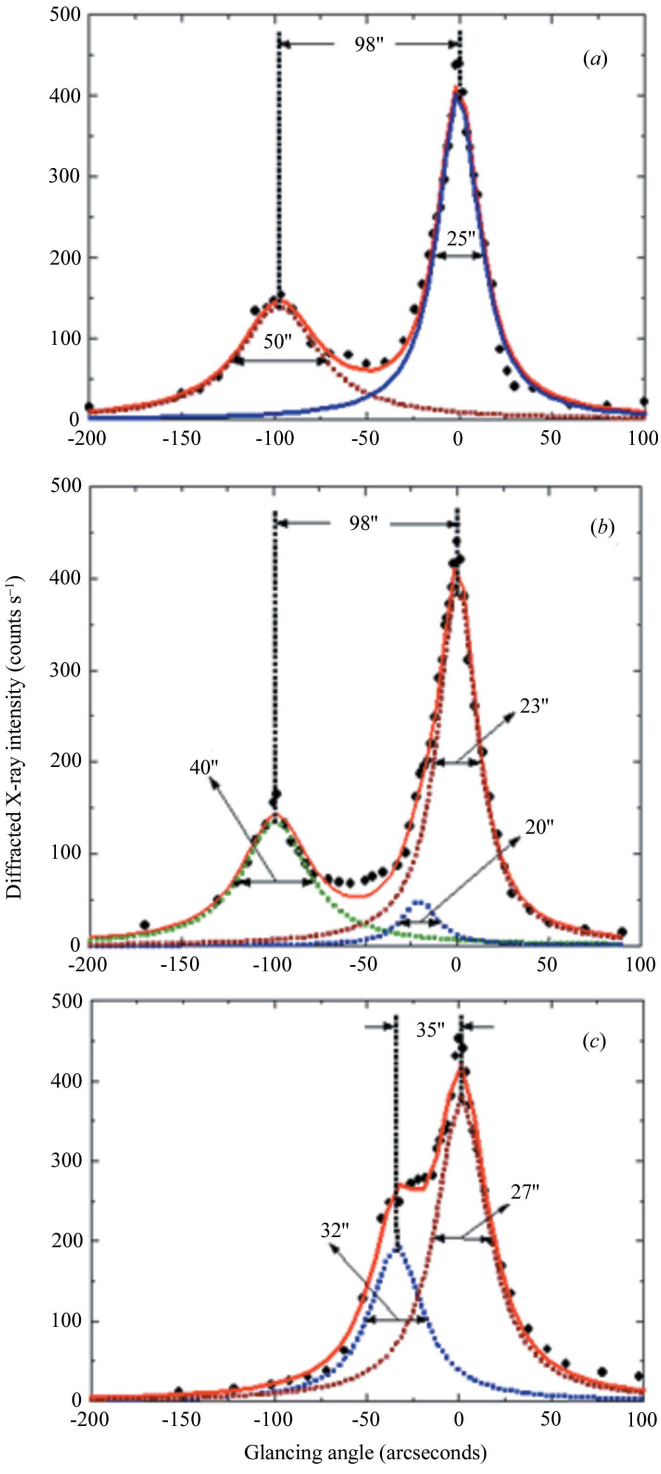

Figure 3
HRXRD curves for a typical LAM single crystal, (*a*) as grown, and (*b*) and (*c*) annealed at 333 and 353 K, respectively, for 6 h.

Fig. 3(*b*) shows the DC recorded after annealing at 333 K for 6 h. The features are almost same as those of the as-grown crystal. However, some minute differences are present: the FWHM values of both the main crystal block and the low-angle boundary are reduced to 23 and 40 arcseconds, respectively, from their initial values of 25 and 50 arcseconds, showing that the crystalline quality is improved to some extent. Another noteworthy point is that a small peak can be observed after deconvolution, which arises as a result of a small very low angle boundary in between the two prominent crystalline regions. This can be seen in the as-recorded DC as a small hump on the left-hand side of the main peak at nearly half the peak intensity. This may be an indication that some portion of the low-angle boundary tends to orient along the main crystal axis.

The same sample was then further annealed at 353 K for 6 h. Fig. 3(*c*) shows the DC for this sample. Now the differences are more obvious. The main difference is the merging of the two curves. The tilt angle between the peaks is reduced from 98 to 35 arcseconds, revealing the fact that, as a result of annealing at this temperature, the low-angle boundary is able to reorient towards the crystallographic direction of the main crystal block and thus the low-angle boundary becomes a very low angle boundary ($\alpha < 1$ arcminute). As the crystal does not yet have a single structural domain, annealing at temperatures greater than 353 K was tried. However, prolonged heating at relatively higher temperatures caused the crystalline perfection to decrease. It may be mentioned here that such residual very low angle boundaries could be detected with well resolved peaks in the diffraction curve only because of the high resolution of the multicrystal X-ray diffractometer used in the present studies. Indeed, such minute disorder of crystalline perfection may not affect most of the device characteristics. However, for specific applications related to optical and piezoelectric properties, it is better to know such minute crystalline details, as shown in our recent studies on as-grown and annealed lithium niobate single crystals (Bhagavannarayana, Budakoti *et al.*, 2005).

3.3. Second harmonic generation efficiency measurements

The SHG efficiency was measured for the grown and annealed single crystals using the Kurtz & Perry (1968) powder technique as described in §2.2. The relative SHG efficiencies for the as-grown (303 K) and 333 K annealed specimens were found to be 0.32 and 0.33 times that of KDP, but at the 353 K annealing temperature the efficiency was increased significantly and was found to be 1.54 times higher than that of the KDP crystals. A comparison of the SHG

efficiencies is shown in Fig. 4. The SHG values are in tune with the crystalline perfection.

3.4. Optical studies

3.4.1. UV–vis–NIR spectroscopy. The recorded UV–vis–NIR transmission spectrum for LAM in the wavelength range 200–1100 nm is shown in Fig. 5, from which it is clear that LAM has good optical transparency in the complete UV–vis region and the optical transparency of the crystal is increased with annealing. The lower cut-off wavelength is found to be around 230 nm, which is far below the SHG output wavelength from the crystal. Hence it is optically transparent, which is a prerequisite for laser applications.

3.4.2. Fluorescence studies. The emission spectra of the as-grown and annealed single crystals of LAM were recorded in the range 500–800 nm as shown in Fig. 6. The samples were excited at 300 nm. A peak at about 564 nm was found in the emission spectra for as-grown and annealed crystals. This result indicates that the LAM single crystal has green fluorescence emission. As seen in the figure, the FL intensity is enhanced as a result of annealing and is maximum at an annealing temperature of 353 K, at which the maximum improvement in the crystalline perfection of the LAM crystal was observed by the HRXRD studies.

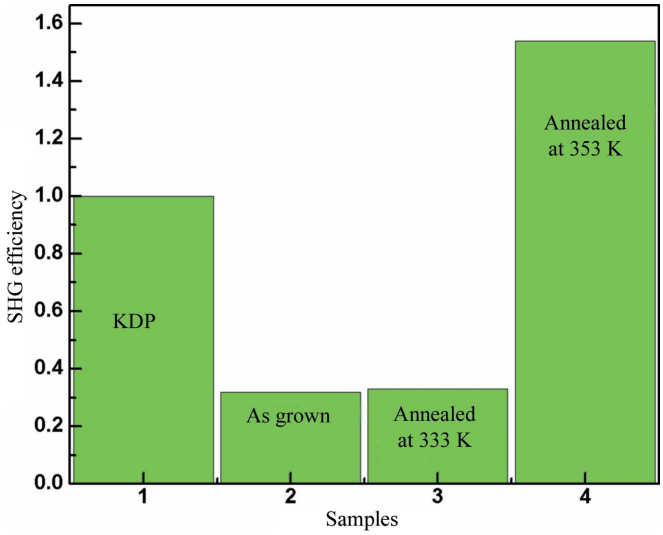

Figure 4
SHG efficiency of KDP, as-grown and annealed LAM crystals.

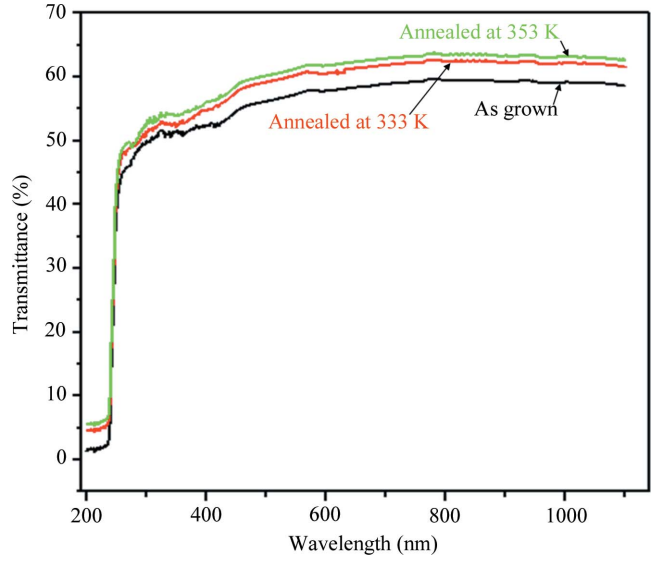

Figure 5
UV–vis transmission spectra of as-grown and annealed LAM crystals.

3.5. Dielectric studies

Dielectric properties are interconnected with the electro-optic properties of a crystal (Boomadevi & Dhanasekaran, 2004), particularly for nonconducting materials. An optical material with high dielectric constant requires a larger poling voltage in order to polarize the dipoles and can suffer changes in the refractive index. The title organic material has a low dielectric constant, eliminating the need for poling while maintaining the refractive index. Figs. 7(*a*) and 7(*b*) depict ε_r and $\tan\delta$, respectively, as a function of frequency. It is clear from Fig. 7(*a*) that the room-temperature values of ε_r gradually decrease as the frequency is increased. The dipolar, ionic, space charge and electronic polarizations all contribute in the low-frequency region (Rajanrajan *et al.*, 2007). However, as the temperature increases, ε_r decreases up to ~75 kHz but increases above 100 kHz. To show clearly the difference in the dielectric constant at different temperatures, the lower part of the graph is expanded in the *y*-axis direction and given in the same figure (Fig. 7*a*). These features indicate that, at low frequencies, the dipolar contribution to the total polarizability of the LAM specimen decreases as the temperature increases, whereas at high frequencies, the electronic contribution increases (Kushwaha *et al.*, 2008). The $\tan\delta$ plot (Fig. 7*b*) indicates that the loss factor decreases with frequency at all temperatures. The values of $\tan\delta$ gradually decrease with respect to temperature in the entire frequency range. The variation of $\tan\delta$ with temperature is much more prominent at lower frequencies than that at higher frequencies. Such

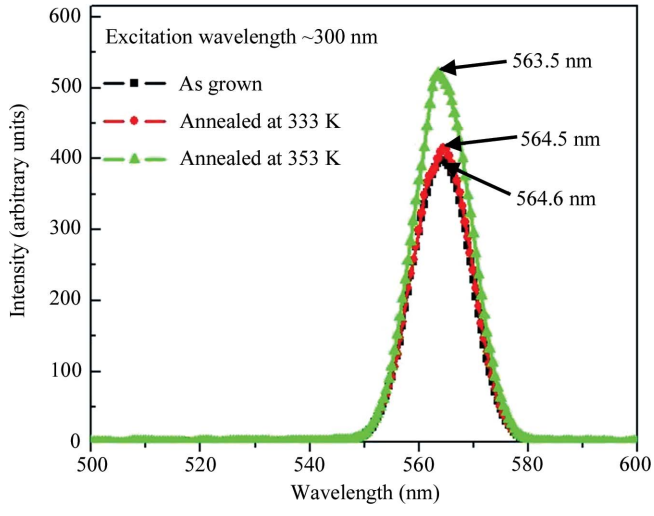

Figure 6
Fluorescence spectra of as-grown and annealed LAM crystals.

variations at high temperature may be attributed to the blocking of charge carriers at the electrodes. Because of the impedance to their motion, space charge and macroscopic distortion result, which might cause the observed larger values of dielectric constant at lower frequencies. With increasing temperature, a high degree of dispersion in the permittivity begins to occur at lower frequencies. It is in fact the space charge effect that leads to the dispersion of the dielectric constant at low frequencies (Rao & Smakula, 1965). The characteristic of low dielectric constant and dielectric loss at high frequencies for a given sample suggests that the sample possesses enhanced optical quality with fewer defects, and this parameter is of vital importance for various nonlinear optical materials and their applications (Balarew, 1984). These dielectric properties of specimens with a very low density of defects are in tune with the HRXRD studies.

The alternating current (a.c.) conductivity of the crystals has been evaluated according to the formula $\sigma_{ac} = \varepsilon_0 \varepsilon_r 2\pi \nu \tan\delta$, where ε_0 is the vacuum dielectric constant, ε_r is the dielectric constant for the LAM crystal and ν is the frequency of the applied a.c. field. The variation of σ_{ac} with frequency at different temperatures is shown in Fig. 8. It is seen that the a.c. conductivity remains almost constant up to 10 kHz, increases slightly in the mid-frequency range (10–100 kHz) and increases rapidly at higher frequencies (up to 1.0 MHz). These variations in the a.c. conductivity may be due to the hopping mechanism, which occurs in the presence of the field applied to the specimen, and follow a power law governed by the expression (Akgul *et al.*, 2008; Singh *et al.*, 2007)

$$\sigma(\nu) \propto A\nu^{s} \quad (1)$$

where A is a constant and s is the exponent, whose value depends on the temperature. The value of s has been calculated from log–log plots of a.c. conductivity *versus* frequency at different temperatures. For a particular temperature, its value remains almost constant. At room temperature, it is around 0.9. This value is gradually and slightly reduced with increasing temperature, reaching 0.8 when the temperature reaches 353 K.

4. Conclusions

L-Asparagine monohydrate single crystals have been grown successfully by the SEST method. The structure has been confirmed by powder XRD. The crystalline perfection of the grown crystals was studied by HRXRD. The quality of the grown crystals was found to be enhanced by thermal annealing. The low-angle boundaries observed in the as-grown crystals were converted to very low angle boundaries as a result of prolonged annealing at low temperature. The SHG efficiency for the as-grown and annealed (at 333 K) single crystals was, respectively, found to be 0.32 and 0.33 times that of KDP. At relatively higher annealing temperature (353 K) where the crystalline perfection was found to be the best, SHG was found to be significantly high, that is, 1.54 times higher than that of KDP. The optical transparency of the grown single crystal and the FL intensity (of green fluorescence light) were also found to be increased with annealing temperature. An extensive study of dielectric constant and dielectric loss or a.c. conductivity has been made over a wide range of frequencies and at different temperatures. An increase in the dielectric

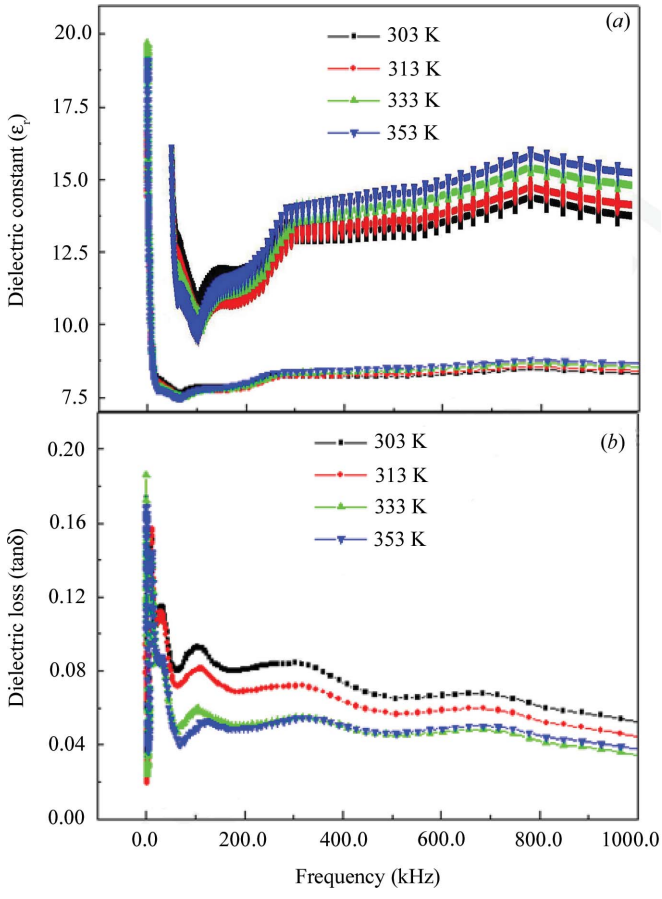

Figure 7
Behavior of (*a*) the dielectric constant and (*b*) dielectric loss of LAM single crystals for the frequency range 100 Hz–1.0 MHz at temperatures of 303, 313, 333 and 353 K.

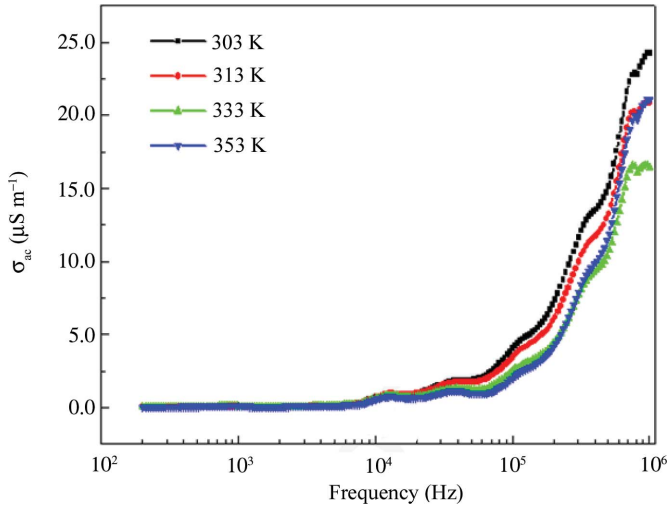

Figure 8
Variation of a.c. conductivity with frequency for the LAM single crystal at temperatures of 303, 313, 333 and 353 K.

constant and a decrease in dielectric loss at higher frequencies were observed. The a.c. conductivity remains almost constant at low frequencies, and then increases slightly in the mid-frequency range and rapidly at higher frequencies, which could be explained on the basis of the correlated barrier hopping model. The main conclusion reached from the present investigation is that even in organic crystals, which generally decompose easily, low-temperature annealing is an effective method to enhance the crystalline perfection, which in turn leads to the enhancement of many physical properties such as SHG, optical and dielectric.

The authors are thankful to the Director, NPL, for his constant encouragement and the necessary support provided for this work. MS acknowledges UGC for providing a fellowship for PhD work. The authors also acknowledge Professor P. K. Das (IISc, Bangalore) for SHG measurements, Dr M. Deepa, NPL, for UV–vis data and Dr T. D. Senguttuvan, NPL, for providing fluorescence spectra.

References

Akgul, U., Ergin, Z., Sekerci, M. & Atici, Y. (2008). *Vacuum*, **82**, 340–345.

Badan, J., Hierle, R., Perigaud, A., Zyss, J. & Williams, D. J. (1993). Editors. *NLO Properties of Organic Molecules and Polymeric Materials*, American Chemical Symposium Series Vol. 233. Washington, DC: American Chemical Society.

Balarew, C. & Dushlew, R. (1984). *J. Solid State Chem.* **55**, 1–6.

Batterman, B. W. & Cole, H. (1964). *Rev. Mod. Phys.* **36**, 681–717.

Bhagavannarayana, G., Ananthamurthy, R. V., Budakoti, G. C., Kumar, B. & Bartwal, K. S. (2005). *J. Appl. Cryst.* **38**, 768–771.

Bhagavannarayana, G., Budakoti, G. C., Maurya, K. K. & Kumar, B. (2005). *J. Cryst. Growth*, **282**, 394–401.

Boomadevi, S. & Dhanasekaran, R. (2004). *J. Cryst. Growth*, **261**, 70–76.

Dong, C. (1999). *J. Appl. Cryst.* **32**, 838.

Krambrock, K., Guedes, K. J., Ladeira, L. O., Bezerra, M. J. B., Oliveira, T. M., Bezerra, G. A., Cavada, B. S., de Oliveira, M. C. F., Flores, M. Z. S., Farias, G. A. & Freire, V. N. (2007). *Phys. Rev. B*, **75**, 104205.

Kripal, R. & Singh, P. (2007*a*). *Solid State Commun.* **142**, 412–416.

Kripal, R. & Singh, P. (2007*b*). *Physica B*, **387**, 222–226.

Kurtz, S. K. & Perry, T. T. (1968). *J. Appl. Phys.* **39**, 3798–3813.

Kushwaha, S. K., Vijayan, N. & Bhagavannarayana, G. (2008). *Mater. Lett.* **62**, 3931–3933.

Lal, K. & Bhagavannarayana, G. (1989). *J. Appl. Cryst.* **22**, 209–215.

Lund, P. (1981). *Nitrogen Metabolism in Mammalian*. Barking: Applied Science.

Misoguti, L., Varela, A. T., Nunes, F. D., Bagnato, V. S., Melo, F. E. A., Mendes Fiho, J. & Zilio, S. C. (1996). *Opt. Mater.* **6**, 147–152.

Moreno, A. J. D., Freire, P. T. C., Guedes, I., Melo, F. E. A., Mendes-Filho, J. & Sanjurjo, J. A. (1999). *Braz. J. Phys.* **29**, 380–387.

Pan, J., Zhang, G., Zheng, Y., Lin, J. & Xu, W. (2007). *J. Cryst. Growth*, **308**, 89–92.

Rajanrajan, K., Mani, G., Vetha Potheher, I., Jesudurai, J. G. M., Vimalan, M., Christy, D., Madhavan, J. & Sagayaraj, P. (2007). *J. Phys. Chem. Solids*, **68**, 2370–2375.

Rao, K. V. & Smakula, A. (1965). *J. Appl. Phys.* **36**, 2031–2038.

Singh, G., Goyal, N., Saini, G. S. S. & Tripathi, S. K. (2007). *J. Non-Cryst. Solids*, **353**, 1322–1325.

Vijayan, N., Bhagavannarayana, G., Maurya, K. K., Pal, S., Datta, S. N., Gopalakrishnan, R. & Ramasamy, P. (2007). *Cryst. Res. Technol.* **42**, 195–200.

Vijayan, N., Bhagavannarayana, G., Ramesh Babu, R., Gopalakrishnan, R., Maurya, K. K. & Ramasamy, P. (2006). *Cryst. Growth Des.* **41**, 784–789.

Verbist, J. J., Lehmann, M. S., Koetzle, T. F. & Hamilton, W. C. (1972). *Acta Cryst.* B**28**, 3006–3013.

Williams, D. J. (1984). *Angew. Chem. Int. Ed. Engl.* **23**, 690–703.

Zaitseva, N. & Carman, L. (2001). *Prog. Cryst. Growth Charact.* **43**, 1–118.